

Weierstraß-Institut für Angewandte Analysis und Stochastik

im Forschungsverbund Berlin e.V.

Preprint

ISSN 0946 – 8633

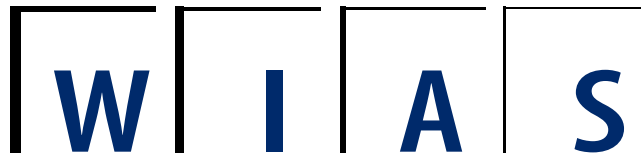
Stochastic flow simulation in 3D porous media

Dmitry Kolyukhin¹ and Karl Sabelfeld^{1,2}

¹ Weierstrass Institute for Applied
Analysis and Stochastics
Mohrenstraße 39
D – 10117 Berlin
Germany
E-Mail: sabelfeld@wias-berlin.de

² Institute of Computational Mathematics
and Mathematical Geophysics
Russian Acad. Sci.
Lavrentieva str., 6
630090 Novosibirsk
Russia

No. 1007
Berlin 2005



1991 *Mathematics Subject Classification.* 65C05, 76N20.

Key words and phrases. Stochastic hydraulic conductivity, Lognormal random field, Darcy law, Randomized spectral representation, Lagrangian statistics, Mean squared separation.

This work is supported partly by the RFBR Grant N 03-01-00914, [HIII](#) N 1271.2003.1, and NATO Linkage Grant N 978912.

Edited by
Weierstraß-Institut für Angewandte Analysis und Stochastik (WIAS)
Mohrenstraße 39
10117 Berlin
Germany

Fax: + 49 30 2044975
E-Mail: preprint@wias-berlin.de
World Wide Web: <http://www.wias-berlin.de/>

Abstract

Stochastic models and Monte Carlo algorithms for simulation of flow through porous media beyond the small hydraulic conductivity fluctuation assumptions are developed. The hydraulic conductivity is modelled as an isotropic random field with a lognormal distribution and prescribed correlation or spectral functions. It is sampled by a Monte Carlo method based on a randomized spectral representation. The Darcy and continuity equations with the random hydraulic conductivity are solved numerically, using the successive over relaxation method in order to extract statistical characteristics of the flow. Hybrid averaging is used: we combine spatial and ensemble averaging to get efficient numerical procedure.

We provide some conceptual and numerical comparison of various stochastic simulation techniques, and focus on the prediction of applicability of the randomized spectral models derived under the assumption of small hydraulic conductivity fluctuations.

1. Introduction

The porosity study has received renewed attention in recent years. Motivations for studying porosity came from many applied fields, in particular, from material science, biomedicine, geology, environment, etc. Simulating flows in natural porous media such as soils, aquifers, oil and gas reservoirs is drastically complicated by the extreme heterogeneities and with insufficient data characterizing the medium.

Generally the porous media is characterized by high irregularities of the size and the form of pores. To approximate the corresponding flow equations, a huge number of nodes is required to get practically relevant results. It should be noted that a reasonable description of the hydraulic conductivity behaviour by a deterministic function meets with serious difficulties. Therefore, a natural choice used in this field is the statistical description of the hydraulic conductivity via random field with a given statistical structure.

Random fields provide a useful mathematical framework for representing disordered heterogeneous media in theoretical and computational studies. Another example is in turbulent transport, where the velocity field representing the turbulent flow is modelled as a random field with statistics encoding important empirical features, and the temporal dynamics of the position of immersed particles is then governed by equations involving this random field, see e.g., [21], [31],[36].

Freeze [10] has analyzed the available data and has found out, that the field of hydraulic conductivity is well described by the random lognormal distribution. In hydrogeology this approach is often used for the flow analysis in saturated zone, or for the transport of a dissolved pollutant in a saturated aquifer [34], [35], [11], [22], [12], [6], [1], [38]. See also the overview in the books [3], [8] and [13].

Generally when dealing with boundary value problems for PDEs with random parameters, one uses two main instruments to analyse the statistical characteristics of the solution: the small perturbation method (based on first- or higher order approximation) applied in the case of small parameter fluctuations, and the direct numerical solution of PDEs for the given samples of the random inputs.

The methods derived in the first order approximation under small hydraulic conductivity fluctuation assumption are used widely [2], [12]. However they have strong restrictions, and as a rule, the applicability conditions are uncertain. Therefore it is important to develop a general direct numerical method which is able to provide calculations beyond the small fluctuation assumptions; in addition, it can be used to validate the small perturbation results. On the other hand, the results obtained by the first approximation method are very useful since they are explicit, and can be therefore used as a benchmark for testing the complicated direct numerical method.

In [29] we have constructed a randomized spectral model (RSM) for simulation of a steady flow in porous media in 3D case under small fluctuation assumptions. The method follows the scheme: first we derive explicitly the spectral tensor of the velocity from that of the hydraulic conductivity; then we construct a Monte Carlo simulation technique for the random velocity with the derived spectral tensor.

Note that a small perturbation analysis using a simulation formula inspired by [17], based on a numerical evaluation of the random field representation through the spectral measure, was applied also in Schwarze et al. [32]. In this approach, when constructing the realizations of random field, the wave vectors are sampled in the whole space. This may cause a poor statistics representation for large wave vectors which in turn may lead to large errors for small scale evaluations like the mean squared separation of two particles. We suggest a different simulation technique which uses a stratified sampling of wave vectors described in [21] and further developed in [18].

Concerning the higher order corrections of the spectral expansion method, we mention that Dagan [7] derived a second-order correction of the head covariances in 3D case. He noted that the first-order approximation is very robust even for a log-conductivity variance equal to unity, the second-order correction of the head variance is smaller than 10% of the first-order approximation. Thus, for small to moderate values of σ_f^2 , it is suggested that the first-order approximation is accurate enough. A similar research for the velocity covariance has been carried out in [9]. These authors explored the accuracy of the first order approximation and reported that for $\sigma_f^2 \ll 1$, the second order corrections to the velocity covariance are unimportant, but as σ_f^2 approaches unity they become significant.

We mention a high-order perturbation approach via Karhunen-Loeve decomposition reported in [39]. In this method, the log hydraulic conductivity Y is decomposed into an infinite series on the basis of a set of non-correlated gaussian standard random variables. The coefficients of the series are related to eigenvalues and eigenfunctions of the covariance function of the log hydraulic conductivity. The advantage of this method is that it suggests an approximation up to fourth-order in σ_Y . However its practical use is limited by the need to solve the complicated eigenvalue problem.

In the general case when the fluctuations are not small, the only rigorous way to tackle the problem is the direct numerical simulation which allows to analyze flows in complex domains though it demands large computing resources.

There are some attempts to develop direct numerical simulation for the problem of transport in porous media. In [34] and [35] an analysis of one- and two-dimensional steady groundwater flows in bounded domain is carried out. The modelling domain has a block structure with a prescribed correlations of the hydraulic conductivity in the neighboring blocks.

Thus for such a simple piecewise-constant approximation of the hydraulic conductivity the authors [34], [35] solved the Darcy equation by a finite-difference method to get samples of the hydraulic potential. It should be noted that their method neither guaranties homogeneity of the generated fields nor a specified correlation structure. An improved version based on a direct matrix inversion method is used in [4] which however is still time consuming.

Another attempt to construct a model of three-dimensional stationary saturated flow beyond the small hydraulic conductivity fluctuations assumption has been made in [1]. In this paper, the estimation of the head variance has been calculated and a comparison with the first order approximation results was carried out. However the authors faced with the demand of large computer resources: it was concluded that to obtain reasonable computational results, the domain and the number of nodes should be increased up to an unrealistic level (about 10^6 nodes).

Statistical characteristics of the velocity field were estimated by direct numerical simulation also in [19] where the authors have developed a stochastic Lagrangian model for the transport in a statistically isotropic porous medium. However the accuracy in these simulations also was not high enough to make definite conclusions desired.

The applicability of the first-order approximation models for the velocity covariance in the mean flow direction in the two-dimensional case was examined in [14]. It was found that these models give very accurate results for the longitudinal velocity covariance for the values of σ_f up to unity. However, the transversal velocity covariance deviates from the direct numerical simulation results as σ_f approaches unity.

Chin and Wang [5] used Monte Carlo simulation for a three-dimensional flow to investigate the accuracy of the first-order approximation, in relation to the Eulerian-Lagrangian covariance relationship. They have used the turning bands algorithm due to Thompson et al. [37]. This method superimposes independent random processes constructed along lines; this is a kind of projection methods constructed from the one-dimensional spectral representations. It also cannot be considered as an efficient simulation method, and in [5] the authors had to restrict the calculations on a crude mesh.

In this paper we develop a direct simulation model in three dimensions which is based on a numerical evaluation of the random realizations of the hydraulic conductivity by the successive over relaxation method (DSM-SOR method). The samples of the hydraulic log-conductivity are constructed by a randomized spectral method. Since the DSM-SOR method works for arbitrary large fluctuations we are able to investigate the applicability of the models derived in the first order approximation. The results extracted from the numerical simulations are also useful for the parametrization of the Lagrangian stochastic model developed in [19].

Note that both in DSM-SOR method and in the first order approximation approach, we use the randomized spectral method to simulate the random fields with the desired

spectral tensor. Hence, the construction of an efficient random field simulation method is a very important issue in this study.

Interesting insights into the dynamics of transport in disordered media can be achieved already through relatively simple random models for the velocity field, such a finite superposition of Fourier modes, with each amplitude independently evolving according to an Ornstein-Uhlenbeck process [26, 33]. We will use instead randomized spectral methods for scalar and vector gaussian fields described in [30] and further developed in [18].

The paper is organized as follows. We start by formulating the stochastic boundary value problem in section 2. The DSM-SOR method is described in section 3. The first order approximation and the relevant randomized spectral model are presented in section 4. Section 5 includes calculations aimed at testing the DSM-SOR method by comparing with the results obtained by the randomized spectral model under small fluctuation assumptions. The main numerical simulation results obtained by DSM-SOR method for the general case of hydraulic conductivity fluctuations are presented in section 6.

2. Formulation of the problem

We consider a steady flow through saturated porous formation. For a stationary 3D flow, the specific discharge is determined by the Darcy law

$$\mathbf{q}(\mathbf{x}) = \theta(\mathbf{x})\mathbf{u}(\mathbf{x}) = -K(\mathbf{x})\nabla(\varphi(\mathbf{x})), \quad \mathbf{x} \in D \subset \mathbb{R}^3 \quad (2.1)$$

where \mathbf{q} is the so-called Darcy's velocity, or specific discharge, \mathbf{u} is the pore velocity, θ , the porosity, φ , the hydraulic potential $\varphi = \frac{p}{\rho g} + z$, p is the fluid pressure, z is the height, and K is the hydraulic conductivity assumed to be a homogeneous lognormal random field with a given spectral density.

Thus \mathbf{q} is a random field defined by (2.1) where φ is the solution of the following conservation of mass equation

$$\sum_{j=1}^3 \frac{\partial}{\partial x_j} \left(K(\mathbf{x}) \frac{\partial \varphi}{\partial x_j} \right) = 0. \quad (2.2)$$

The functions K and θ are the key parameters of the flow. Experimental measurements show a high heterogeneous behaviour of K in space with the following remarkable property: when considering K as a random field, its distribution is well approximated by a log-normal law (e.g., see [10]).

The porosity θ is also often considered in some models as a random field. However its variability is in the problems we tackle generally much smaller than that of K . We assume therefore $\theta(\mathbf{x}) = \theta = \text{const}$.

We will consider the hydraulic log-conductivity $\ln K = F + f$ as a statistically homogeneous random field with gaussian distribution $N(m_f, \sigma_f)$. Here $m_f = F$ is the mean, and σ_f is the standard deviation. We denote by

$$C_{ff}(\mathbf{r}) = \langle f(\mathbf{x})f(\mathbf{x} + \mathbf{r}) \rangle$$

the auto-correlation function, where \mathbf{r} is the separation vector.

Moreover we assume first that f is statistically homogeneous and isotropic with the exponential auto-correlation function

$$C_{ff}(r) = \sigma_f^2 \exp(-r/I_f) , \quad (2.3)$$

where $r = |\mathbf{r}|$, I_f is a given correlation length.

The equation (2.2) will be solved in a finite domain, with the relevant boundary value conditions formulated in the next section.

3. Direct numerical simulation method: DSM-SOR

In this section we present the direct simulation method based on the successive over relaxation iterative solution of the relevant PDE. For brevity, we will call it DSM-SOR method.

In numerical simulations we deal with the following boundary value problem in the domain $D = [0 : L_1] \times [0 : L_2] \times [0 : L_3]$:

$$\sum_{j=1}^3 \frac{\partial}{\partial x_j} \left(K(\mathbf{x}) \frac{\partial \varphi}{\partial x_j} \right) = 0 , \quad (3.1)$$

with the constant head (on the left and right bounds: $x_1 = 0$ and $x_1 = L_1$) and impervious (on other bounds of the domain D) boundary conditions:

$$\left\{ \begin{array}{ll} \varphi(\mathbf{x}) = \varphi_0 & , \quad x_1 = 0 \\ \varphi(\mathbf{x}) = \varphi_0 - \mathbf{J}L_1 & , \quad x_1 = L_1 \\ \frac{\partial \varphi(\mathbf{x})}{\partial n} = 0 & , \quad x_2 = 0, x_2 = L_2, x_3 = 0, x_3 = L_3 \end{array} \right. . \quad (3.2)$$

Here $J_j = -\partial\langle\varphi\rangle/\partial x_j$ is the mean hydraulic gradient in x_j -direction, $\mathbf{J} = (J_1, J_2, J_3)$ is taken in this paper as a constant vector $\mathbf{J} = (J, 0, 0)$, and φ_0 being a constant. The hydraulic log-conductivity $\ln K$ is assumed to be a gaussian isotropic random field with the mean $F = 3.4012$ and the auto-covariance (2.3).

To construct the solution of the equation (3.1), for a chosen sample of $K(x)$ and satisfying the boundary conditions (3.2) we use the following finite-difference scheme in the interior nodes [16]

$$\left[K_{i-\frac{1}{2}jl} + K_{i+\frac{1}{2}jl} + K_{ij-\frac{1}{2}l} + K_{ij+\frac{1}{2}l} + K_{ijl-\frac{1}{2}} + K_{ijl+\frac{1}{2}} \right] \varphi_{ijl} - K_{i-\frac{1}{2}jl} \varphi_{i-1jl} \\ - K_{i+\frac{1}{2}jl} \varphi_{i+1jl} - K_{ij-\frac{1}{2}l} \varphi_{ij-1l} - K_{ij+\frac{1}{2}l} \varphi_{ij+1l} - K_{ijl-\frac{1}{2}} \varphi_{ijl-1} - K_{ijl+\frac{1}{2}} \varphi_{ijl+1} = 0$$

with the uniform grid $h_1 = h_2 = h_3 = h$.

The normal derivative on the boundary was approximated by simply using the first order approximation along the normal vector.

The finite-difference scheme can be written in a matrix form

$$A\varphi_h = (\text{Diag}(A) - L - U)\varphi_h = f_h \quad (3.3)$$

where φ_h is the approximating solution vector which depends on the indexation, f_h is the vector in the right-hand side; $\text{Diag}(A)$ is the diagonal matrix whose entries coincide with the diagonal elements of the matrix A ; analogously, L and U are the left and right triangular matrices extracted from the matrix A . We use the successive over relaxation (SOR) iterative method for solving (3.3):

$$\varphi_h^n = w[\text{Diag}(A)]^{-1}(f_h + L\varphi_h^n + U\varphi_h^{n-1} + (1 - w)\varphi_h^{n-1}) .$$

In [27], [28], the influence of boundary conditions in a two-dimensional case was investigated. It was shown that beyond 3 or 4 correlation lengths (for constant head boundary conditions, or even less for impervious boundary conditions) the influence of boundary effects on the second moment of the hydraulic potential can be neglected. The influence of the impervious boundary conditions on the head covariances in three-dimensional flow is quite small and restricted to the neighborhood of the boundary [24], [8]. The head increments are even less sensitive to the boundary conditions. In [19], all the statistical characteristics were calculated in a domain placed 5 correlation lengths far from the head constant or impervious boundaries of the domain D . In our calculations, 4 correlation lengths were enough for correct evaluation of the velocity correlations. Thus we consider two domains: the region $D = [0 : L_1] \times [0 : L_2] \times [0 : L_3]$, and $\tilde{D} = [4I_f : L_1 - 4I_f] \times [4I_f : L_2 - 4I_f] \times [4I_f : L_3 - 4I_f]$. In the region D the equations (2.1), (2.2) are solved numerically by the SOR method, and the desired statistical characteristics are calculated in the domain \tilde{D} .

The hydraulic potential is chosen as $\varphi_0 = 100m$. To reproduce the field K , in [19] is recommended to choose the grid size h at least not larger than $I_f/4$; in [1] this value was recommended as $I_f/5$. We have taken the grid size equal to $h = I_f/5$ and $h = I_f/6$, and the time step was $\Delta t = 0.25h / \langle u \rangle$.

4. Randomized Spectral model (RSM)

In this section we present the randomized spectral model (RSM) applied along with the first order approximation expansion under small fluctuation assumptions. So let us first describe the first order approximation model; small random perturbation about the mean values for the potential, specific discharge and pore velocity components are assumed:

$$\varphi = \langle \varphi \rangle + \varphi' = H + h, \quad q_j = \langle q_j \rangle + q'_j, \quad u_j = \langle u_j \rangle + u'_j, \quad j = 1, 2, 3 .$$

The auto-covariance (2.3) has the spectrum

$$S_{ff}(k) = I_f^3 \sigma_f^2 / [\pi^2 (1 + I_f^2 k^2)^2], \quad (4.1)$$

where $\mathbf{k} = (k_1, k_2, k_3)$ is the wave number vector, and $k = |\mathbf{k}|$.

Under the assumption of small hydraulic conductivity fluctuations the spectrum of specific discharge has the form [12]:

$$S_{q_j q_l}(k) = K_G^2 J_m J_n \left(\delta_{jm} - \frac{k_j k_m}{k^2} \right) \left(\delta_{ln} - \frac{k_l k_n}{k^2} \right) S_{ff}(k) . \quad (4.2)$$

In [29] the randomized simulation approach developed in [30] is used to construct a divergenceless vector field with a given spectral tensor. We have constructed Monte Carlo simulation formulas for the specific discharge perturbation \mathbf{q}' , and hence the velocity perturbation \mathbf{u}' . We simulate $i = 1, 2, \dots, N$ independent random fields with $S(\mathbf{k})$, then we set

$$\mathbf{u}'^{(N)}(\mathbf{x}) = \frac{1}{\sqrt{N}} \sum_{i=1}^N \left[\frac{1}{\sqrt{p(\mathbf{k}_i)}} \left(\xi'_{ki}(\mathbf{a}) \cos(\mathbf{k}_i, \mathbf{x}) + \eta'_{ki}(\mathbf{a}) \sin(\mathbf{k}_i, \mathbf{x}) \right) \right] ,$$

where

$$\xi'_{ki}(\mathbf{a}) = \xi_{ki} \mathbf{a}(\mathbf{k}) , \quad \eta'_{ki}(\mathbf{a}) = \eta_{ki} \mathbf{a}(\mathbf{k}) ,$$

$$a_j(\mathbf{k}) = \frac{K_G}{\theta} \left(J_j - \frac{k_j J_m k_m}{k^2} \right) (S_{ff}(\mathbf{k}))^{1/2} , \quad j = 1, 2, 3,$$

ξ_{ki} and η_{ki} being random variables with zero mean and unit variance, and \mathbf{k}_i , ξ_{ki} , η_{ki} are all sampled independently. Here \mathbf{k} is sampled according to the density $p(\mathbf{k})$ which is, generally, an arbitrary density function which can be chosen from rather different arguments. For instance, it is recommended in [30], to use $p(\mathbf{k}) = a^2(\mathbf{k}) / \int_{R^3} a^2(\mathbf{k}) d\mathbf{k}$.

The central limit theorem ensures, under some general assumption [20], that $\mathbf{u}'^{(N)}(\mathbf{x})$ converges to an ergodic gaussian random field with the spectral tensor $S(\mathbf{k})$, as $N \rightarrow \infty$.

Under small perturbations assumption, $\langle \mathbf{q} \rangle = K_G \mathbf{J}$ (see [8]), so the velocity is modelled as $\mathbf{u}(\mathbf{x}) = (K_G \mathbf{J}) / \theta + \mathbf{u}'(\mathbf{x})$.

More general randomized spectral simulation method is constructed by introducing a stratified sampling of the wave numbers, see [21] and [18]. Let us present the simulation formula in its general form.

Let $\mathbf{u}(\mathbf{x}) = u_1(\mathbf{x}, \dots, u_l(\mathbf{x}))^T$, $\mathbf{x} \in R^d$ be a homogeneous vector gaussian random field with the given spectral tensor $F(\mathbf{k})$ which is related to the correlation tensor $B(r) = \langle \mathbf{u}(\mathbf{x} + \mathbf{r}) \mathbf{u}^T(\mathbf{x}) \rangle$ by

$$B(r) = \int_{R^d} \exp\{2\pi i \mathbf{k} \mathbf{r}\} F(\mathbf{k}) d\mathbf{k} , \quad F(\mathbf{k}) = \int_{R^d} \exp\{-2\pi i \mathbf{k} \mathbf{r}\} B(\mathbf{r}) d\mathbf{r} . \quad (4.3)$$

Here $()^T$ is used for the notation of transpose operation.

Let

$$p(\mathbf{k}) = \sum_{j=1}^l F_{jj}(\mathbf{k})$$

and assume that $\sigma^2 = \int_{R^d} p(\mathbf{k}) d\mathbf{k} < \infty$.

We will use the Holeski decomposition

$$F(\mathbf{k}) = p(\mathbf{k}) Q(\mathbf{k}) Q^*(\mathbf{k}) , \quad (4.4)$$

where the matrix Q^* is defined as a complex conjugate transposition $Q^* = \overline{Q^T}$.

We denote by Q' and Q'' the real and imaginare parts of the tensor Q : $Q(\mathbf{k}) = Q'(\mathbf{k}) + i Q''(\mathbf{k})$.

Let us denote by $\Delta = \text{supp}(p)$ the support of the spectral density $p(\mathbf{k})$. We choose a subdivision of Δ : $\Delta = \sum_{i=1}^n \Delta_i$.

Let $\mathbf{k}_{i1}, \dots, \mathbf{k}_{in_0}$ be a family of mutually independent identically distributed random points lying in Δ_i sampled from the pdf

$$f_i(\mathbf{k}) = \begin{cases} \frac{p(\mathbf{k})}{\sigma_i^2}, & \mathbf{k} \in \Delta_i, \\ 0, & \text{else} , \end{cases} \quad \sigma_i^2 = \int_{\Delta_i} p(\mathbf{k}) d\mathbf{k} . \quad (4.5)$$

The randomization spectral model can be written in the form

$$\begin{aligned} \mathbf{u}_{nn_0}(\mathbf{x}) = & \sum_{i=1}^n \frac{\sigma_i}{\sqrt{n_0}} \sum_{j=1}^{n_0} \left\{ \xi_{ij} \left[Q'(\mathbf{k}_{ij}) \cos \theta_{ij} - Q''(\mathbf{k}_{ij}) \sin \theta_{ij} \right] \right. \\ & \left. + \eta_{ij} \left[Q''(\mathbf{k}_{ij}) \cos \theta_{ij} + Q'(\mathbf{k}_{ij}) \sin \theta_{ij} \right] \right\} , \end{aligned} \quad (4.6)$$

where $\theta_{ij} = 2\pi \mathbf{k}_{ij} \cdot \mathbf{x}$, and ξ_{ij}, η_{ij} , $i = 1, \dots, n$; $j = 1, \dots, n_0$ are mutually independent and independent of the family \mathbf{k}_{ij} standard l -dimensional gaussian random variables (with zero mean and unity covariance matrix): $\xi_{ij} = (\xi_{ij}^{(1)}, \dots, \xi_{ij}^{(l)})$, $\eta_{ij} = (\eta_{ij}^{(1)}, \dots, \eta_{ij}^{(l)})$.

5. Testing the simulation procedure

In this section we test the direct numerical technique by comparing the results against the calculations obtained by RSM. Obviously RSM is a reasonable approach for small fluctuations, so we compare the results mainly for $\sigma_f^2 = 0.01$, and fix $\theta = 1.0$ and $I_f = 1$. For testing the DNS-SOR method we calculate the correlation functions

$$C_{u_j u_l}(\mathbf{r}) = \langle u_j(\mathbf{x}) u_l(\mathbf{x} + \mathbf{r}) \rangle$$

by the direct numerical simulation based on the SOR iterative procedure, and compare them with the results obtained by the randomized spectral model constructed in [29] for the spectrum (4.2). As concluded in [29], RSM has shown a good agreement with the exact results presented through a numerical integration in the spectral representation

$$C_{u_j u_l}(\mathbf{r}) = \int_{R^3} S_{jl}(\mathbf{k}) e^{i(\mathbf{r}, \mathbf{k})} d\mathbf{k} , \quad (5.1)$$

where Simpson's rule was used to evaluate the integral (5.1). The expectations in RSM were evaluated by averaging over $N = 10^5$ samples.

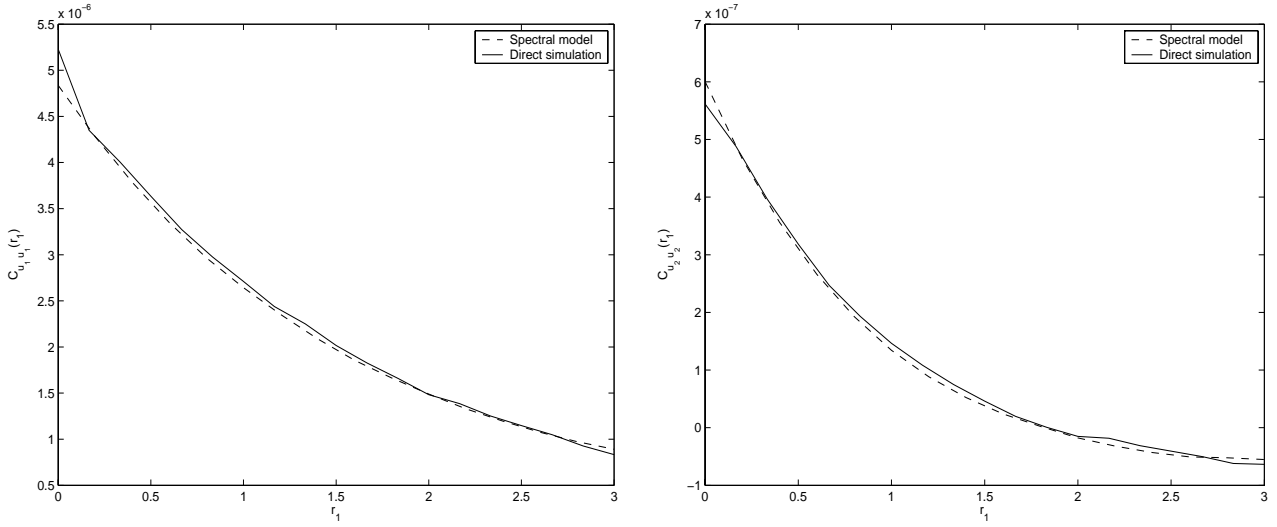


Figure 1: The auto-correlation function $C_{u_1 u_1}(\mathbf{r})$ (left panel) and $C_{u_2 u_2}(\mathbf{r})$ (right panel) in longitudinal direction.

For evaluation of statistical characteristics of a stochastic flow one usually uses two different averaging procedures: (1) space averaging [1], [38], [19], and (2) ensemble averaging [34], [35], [5], [14]. To use the space averaging, we have to be sure that our randomized spectral model has good ergodic properties. As reported in [18], this is the case if the number of harmonics is sufficiently large, say, over one thousand.

A compromise which seeks to avoid the problems of both types of averaging is the hybrid method, or a combined averaging: first the space averaging is taken, and then the result is averaged over n independent samples, n being not so large as in the pure ensemble averaging.

In calculations presented in Fig.1–5 of section 5 we use the ensemble averaging while in section 6 we use the combined averaging.

In Figure 1 we plot the function $C_{u_1 u_1}$ (left panel) and $C_{u_2 u_2}$ (right panel) calculated by the DSM-SOR method (solid lines) and by RSM (dashed lines); both functions are presented for the longitudinal direction r_1 , $J = 0.01$, and the expectation is calculated as an arithmetic mean over $N = 10^4$ samples. The maximal relative difference between the results of two methods for $r_1 = 1$ was 3% for the curves presented in the left panel and 9% in the right panel. The statistical error of the direct simulation results was about 7%, and 12%, respectively; the statistical error of RSM was less than 3%.

The statistical error in calculating an ensemble average of a random estimator ξ was measured by $\varepsilon(\xi) = 3\sigma_\xi/\sqrt{N}$ where σ_ξ^2 is the variance of the random estimator ξ . From Figure 1 it is seen, that the difference between the solid and dashed curves is small everywhere except for small values of the separated vector. This is presumably caused by the limit space resolution of the DSM-SOR method.

To control the space resolution, which is related to the large values of the wave number k in the log-conductivity power spectrum, we introduce a cut-off in the spectrum, so that the spectrum $S_{ff}(\mathbf{k})$ is defined on the interval $[0, k_{max}]$. In Figure 2 we plot similar

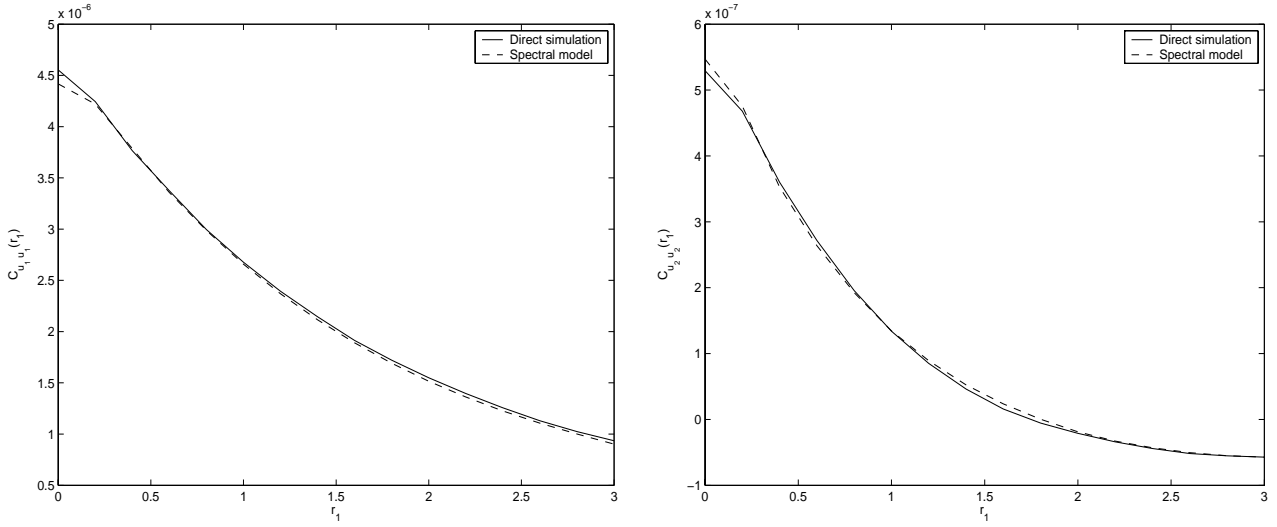


Figure 2: The auto-correlation functions $C_{u_1 u_1}(\mathbf{r})$ (left panel) and $C_{u_2 u_2}(\mathbf{r})$ (right panel) in longitudinal direction. Spectrum $S_{ff}(\mathbf{k})$ is defined on the interval $[0, 15]$.

results for the spectrum (4.1) defined on the interval $[0, 15]$. The total energy of this spectrum is more than 91.5% of the total energy of the full power spectrum on $[0, \infty)$. The relative error (measured as the relative difference with the results obtained by RSM) in calculations of $C_{u_1 u_1}(0)$, $C_{u_2 u_2}(0)$ is decreased from 8% (left panel) and 6.5% (right panel) to 3%. This indicates obviously that for spectra with rapidly decaying tails, we can expect that the accuracy of the direct numerical method will be higher.

Indeed, in [29] we used also a log-conductivity random field with the gaussian form of the covariance

$$C_{ff}(r) = \sigma_f^2 \exp\left(-\frac{r^2}{l_f^2}\right)$$

whose spectrum has also a gaussian form:

$$S_{ff}(\mathbf{k}) = \frac{\sigma_f^2 l_f^3}{\pi^{5/2}} \exp\left(-\frac{l_f^2 k^2}{4}\right), \quad (5.2)$$

where $l_f = l_f \sqrt{\pi}/2$. From Figure 3 it is seen that the velocity field corresponding to this log-conductivity spectrum with $l_f = 1$ is simulated more precisely than in the case of the exponential auto-correlation function (2.3).

As the fluctuations of the hydraulic conductivity are getting smaller ($\sigma_f \rightarrow 0$) then, analogously to the case analysed by RSM, the velocities tend to have gaussian distributions.

In Figures 4,5 the probability density functions of longitudinal and transversal velocities are shown for two different (small and large) values of σ_f . As predicted, for $\sigma_f = 0.01$ the modelled densities (solid lines) are well approximated by gaussian densities (dashed lines) with the mean $\langle u_1 \rangle = K_G J$ and $\sigma_{u_1} = 2.1991392E - 03$, $\sigma_{u_2} = 7.7482074E - 04$ (left panels). For large variance value ($\sigma_f = 1$) the velocity distributions are strongly nongaussian (right panels).

Note that the cross-correlation functions $C_{u_1 u_2}(\mathbf{r})$, $C_{u_2 u_3}(\mathbf{r})$ are identically equal to zero for

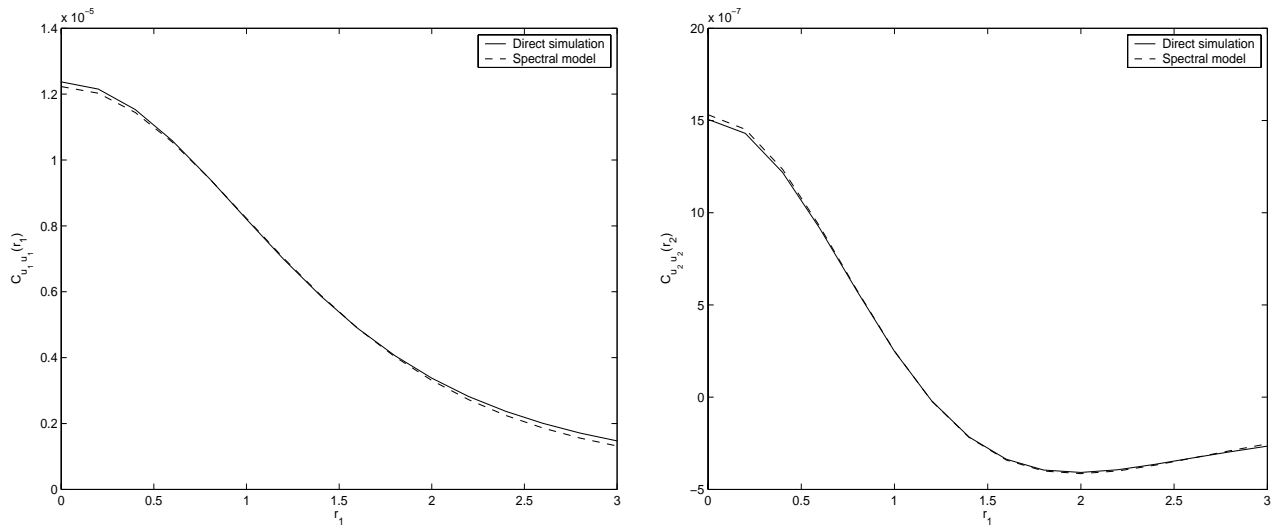


Figure 3: The auto-correlation functions $C_{u_1 u_1}(\mathbf{r})$ (left panel) and $C_{u_2 u_2}(\mathbf{r})$ (right panel) in longitudinal direction; gaussian spectrum $S_{ff}(\mathbf{k})$.

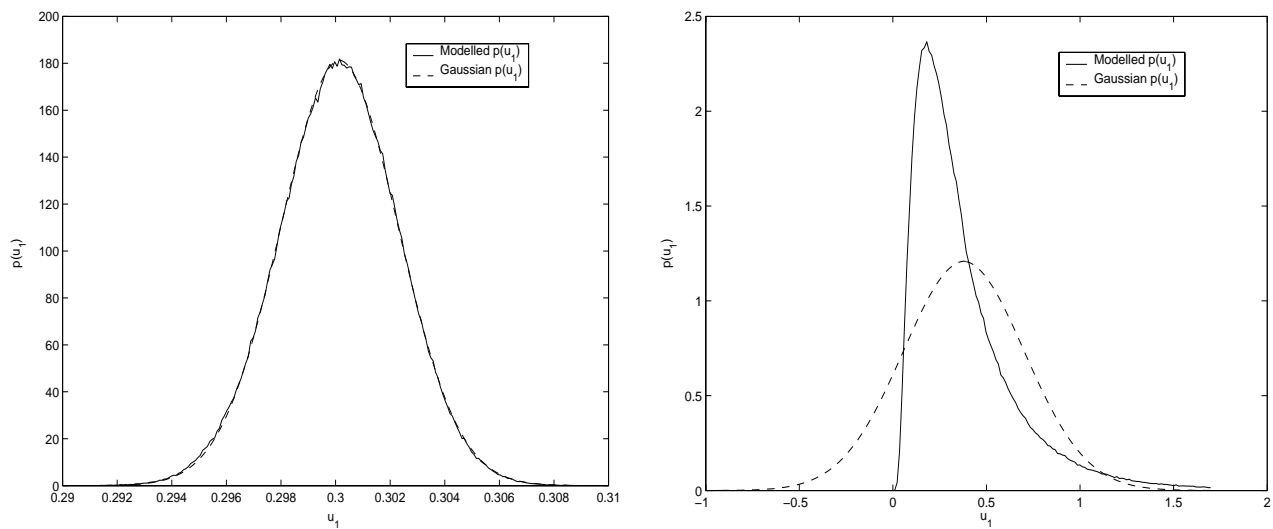


Figure 4: The probability density of longitudinal velocity $p(u_1)$ for $\sigma_f = 0.01$ (left panel) and $\sigma_f = 1$ (right panel).

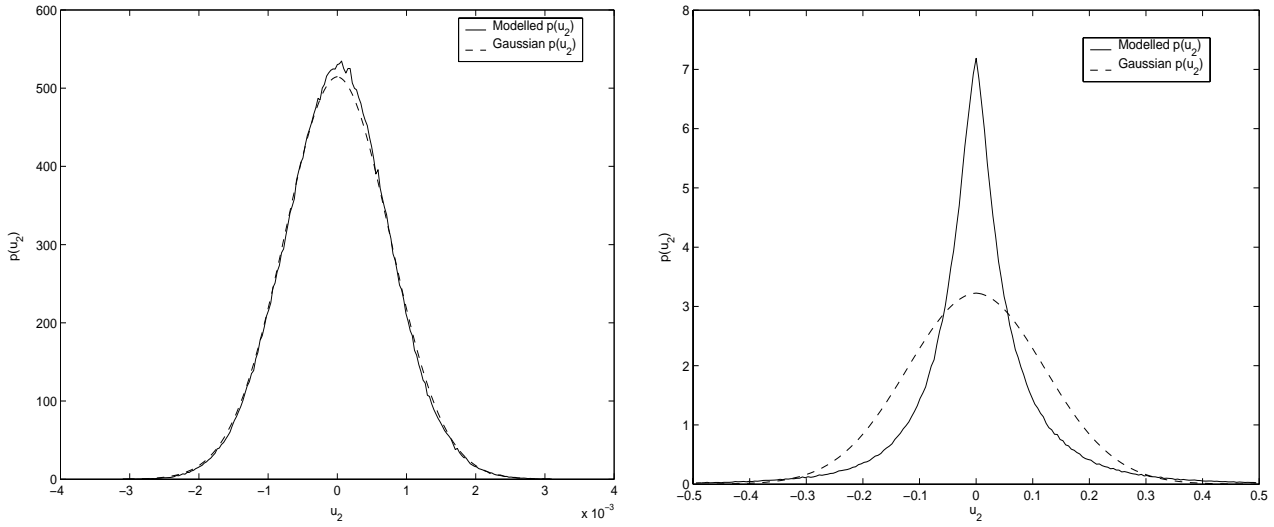


Figure 5: The probability density of transversal velocity $p(u_2)$ for $\sigma_f = 0.01$ (left panel) and $\sigma_f = 1$ (right panel).

arbitrary longitudinal and transversal separated vectors. This property was well confirmed by our calculations.

6. Evaluation of Eulerian and Lagrangian statistical characteristics by DNS-SOR method

In this section we present the results of direct numerical simulation for some Eulerian and Lagrangian statistical characteristics of the flow. The key results are presented in Figure 7 where the Eulerian velocity auto-correlation functions are shown for different intensity fluctuations of the hydraulic conductivity, compared against the results obtained by the randomized spectral method under small fluctuation assumptions. From these curves one easily extracts the region of applicability of the small perturbation approach and RSM. Another important result is presented in Figure 12: here we show the behaviour of the mean square separation of two particles. This complicated two particle Lagrangian statistical characteristic plays a crucial role in the turbulent diffusion study [23]. In the Kolmogorov inertial subrange the behaviour of the mean square separation is described by the well known Richardson's law which predicts a cubic dependence on time. In our case, we cannot extract a universal structure for the function $\rho^2(t)$, not depending on the initial separation. However it has shown an interesting subdiffusion behaviour in transverse direction, and a superdiffusion picture in longitudinal direction.

In the two subsections which follow, we calculate the expectations by the hybrid averaging: we combine spatial and ensemble averaging to get efficient numerical procedure. The Eulerian statistical characteristics were calculated first by spatial averaging over 21^3 nodes, and then by averaging over 300 independent samples of random velocities. The Lagrangian statistical characteristics were calculated by averaging over 252 trajectories per one sample of the random velocity, with subsequent averaging over 400 realizations of the velocity

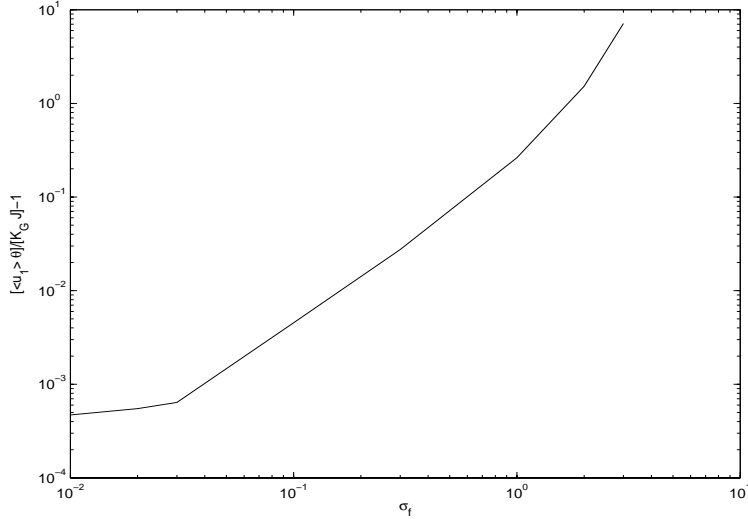


Figure 6: The behaviour of $\frac{\langle u_1 \rangle \theta}{K_G J} - 1$, as a function of σ_f .

field. In all cases, the number of harmonics in the randomized spectral method was taken as $n_0 = 100$.

6.1. Eulerian statistical characteristics

Here we present the results of calculations of the mean Eulerian velocity and velocity auto-correlation functions. The spectrum $S_{ff}(\mathbf{k})$ is chosen in the form (4.1) which corresponds to the exponential decorrelation.

In Figure 6 we plot the mean velocity in a normalized form $\frac{\langle u_1 \rangle \theta}{K_G J} - 1$, for different values of σ_f . This normalization is convenient since the small perturbation method concludes that the mean velocity equals to $K_G J / \theta$.

Note that for $\sigma_f = 1$, our mean longitudinal velocity agrees well with that obtained in [19], being approximately 4% larger. For values of σ_f up to 1.5, the mean velocity was also calculated in [5] where the relative difference with the result predicted by the first order approximation was about 15%. This difference in our calculations was 26%, and 22% - in [19].

Figure 7 shows how good the small perturbation method and RSM work. This can be seen by comparing the RSM results with the data obtained by DSM-SOR method. Here we plot the dimensionless functions $C_{u_1 u_1}$ (left panel) and $C_{u_2 u_2}$ (right panel) in longitudinal direction $r'_1 = r_1 / I_f$, for $\sigma_f = 0.3, 0.6$ and $\sigma_f = 1$. The left panel: as expected, the relative difference between the RSM and DSM-SOR results is rapidly increasing with the growth of the fluctuation intensity, i.e., as σ_f increases. So, for $r'_1 = 1$, this difference behaves like 9%, 29% and 84% for $\sigma_f = 0.3, 0.6$ and 1, respectively. As to the statistical error of these calculations, it was less than 1% for DSM-SOR method, and 2% - for RSM.

Right panel: the relative difference between the two methods (again, for $r'_1 = 1$) is less than 6%, 31% and 108% for $\sigma_f = 0.3, 0.6$ and 1, respectively. The statistical error: less than 2% for DSM-SOR method, and 3% for RSM.

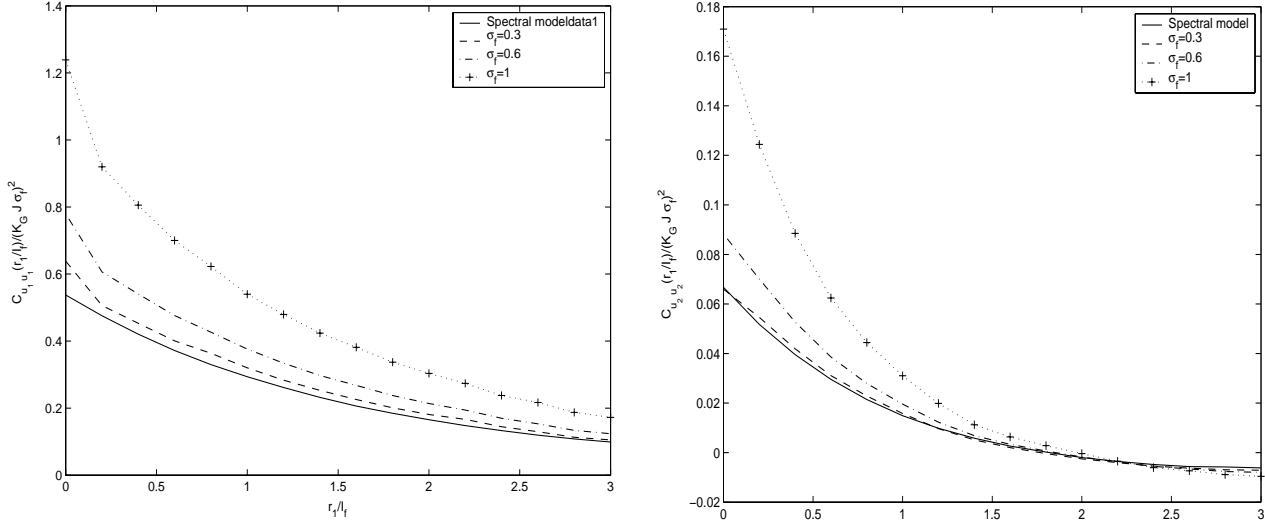


Figure 7: The dimensionless functions $C_{u_1 u_1}(\mathbf{r}/I_f)$ (left panel) and $C_{u_2 u_2}(\mathbf{r}/I_f)$ (right panel) in longitudinal direction at different values σ_f in comparison against results of spectral model.

Thus the curves shown in Figure 7 present a clear picture about the region where the small perturbation approach and RSM can be applied, and how fast this approximation fails as the fluctuation intensity increases.

6.2. Lagrangian statistical characteristics

In this section we present the results of numerical simulations for some Lagrangian statistical characteristics of the flow, $\sigma_f = 1$ is fixed. The calculations were carried out for the exponential correlations controlled by the spectrum (4.1), and by the gaussian correlations with the spectrum (5.2).

The random Lagrangian trajectory $\mathbf{X}(t) = (X_1(t), X_2(t), X_3(t))$ starting at a point \mathbf{x}_0 is defined as a function satisfying the following stochastic equation

$$\frac{d\mathbf{X}}{dt} = \mathbf{u}(\mathbf{X}), \quad \mathbf{X}(0) = \mathbf{x}_0 . \quad (6.1)$$

The displacement covariances are defined by

$$D_{jl}(t) = \langle (X_j(t) - \langle X_j \rangle(t))(X_l(t) - \langle X_l \rangle(t)) \rangle .$$

In what follows we deal with the normalized quantities:

$$D'_{jl} = D_{jl}/I_f^2, \quad j, l = 1, 2, 3 ,$$

and dimensionless time $t' = tU/I_f$, where $U = \langle u_1 \rangle$, and $K_G = exp(F)$.

In Figure 8, the dispersions $D'_{11}(t')/\sigma_f^2$ (left panel), and $D'_{22}(t')/\sigma_f^2$ (right panel) are shown. The curves seem to follow a linear law in time from, say, $t' = 3$ which would be in accordance with the classical Taylor's formula. To confirm this, we have extended these

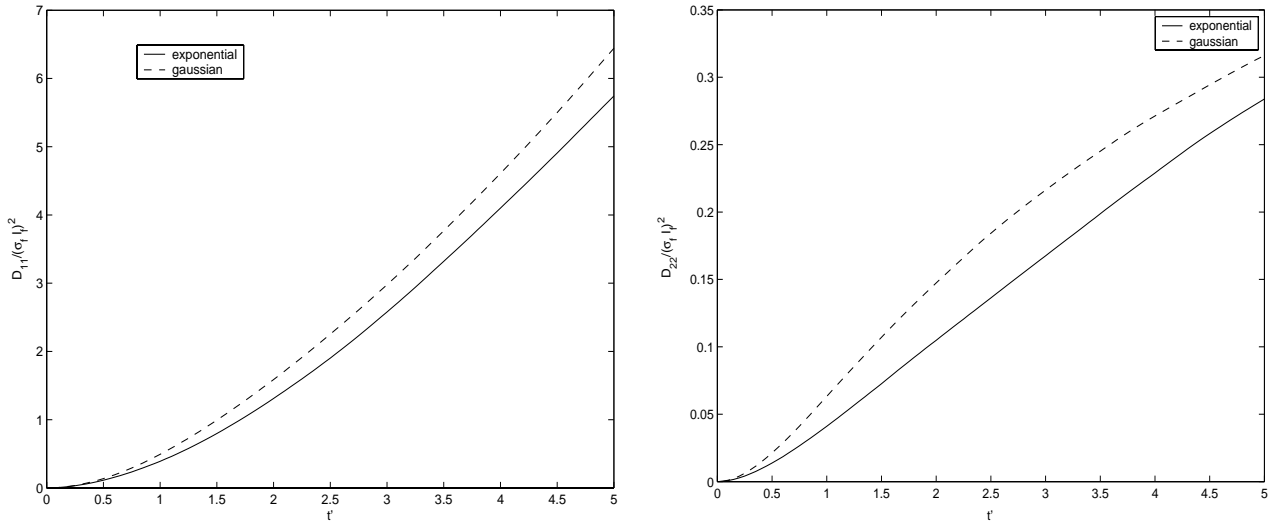


Figure 8: The dimensionless functions $D'_{11}(t')/\sigma_f^2$ and $D'_{22}(t')/\sigma_f^2$ (right panel). Small time.

calculations to the times up to $t' = 30$, see Figure 9. From these results we can conclude that the linear law happens to be true after the time $t' = 5$, both for the longitudinal and transverse dispersions.

Important Lagrangian statistical characteristic is the Lagrangian correlation tensor of velocity:

$$R_{ji}(\tau) = \langle [(u_j(X(t)) - \langle u_j(X(t)) \rangle) [(u_i(X(t + \tau)) - \langle u_i(X(t + \tau)) \rangle)] \rangle$$

where $X(t)$ is a Lagrangian trajectory started at the time t .

In Figure 10 we show the longitudinal (left panel) and transverse (right panel) Lagrangian correlation functions. Note that the transverse correlations have negative values after $t' \approx 1$, which may be connected with a trapping, and which can lead to a deviation from the linear law of the transverse dispersion. To check it, we have calculated (see Figure 11) the integral

$$A_{jj}(\tau) = \int_0^\tau R_{jj}(\tau') d\tau' .$$

These results are in a good qualitative agreement with the results obtained by D. Chin and T. Wang in [5], although their calculations were limited by the grid size $h = I_f/2$ which is too large to provide high accuracy. Thus the D. Chin and T. Wang results underestimate the longitudinal dispersivity (left panel) to about 30%, and the transverse dispersivity - to about 15% compared to our results.

Recall that Taylor's formula relating the dispersion tensor and the Lagrangian velocity covariance

$$D_{ji}(t) = 2 \int_0^t (t - \tau) R_{ji}(\tau) d\tau$$

indicates that for large times, the integral A_{jj} should not vanish (the linear dispersion behaviour for large times). This is confirmed by the calculations presented in Figure 11.

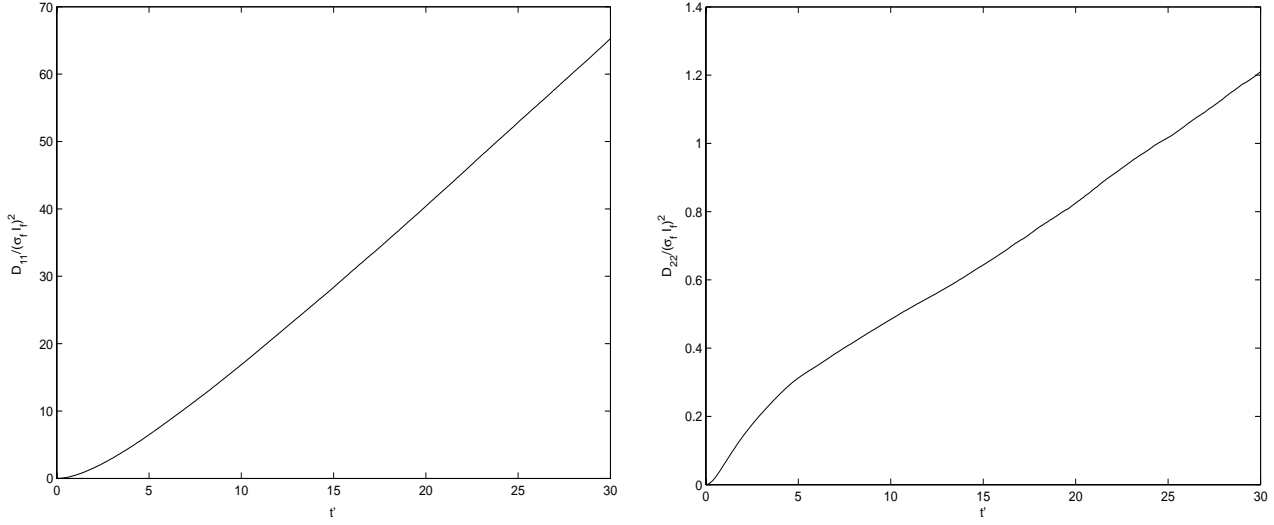


Figure 9: The dimensionless functions $D'_{11}(t')/\sigma_f^2$ and $D'_{22}(t')/\sigma_f^2$ (right panel). Large time. Gaussian spectrum S_{ff} , (5.2).

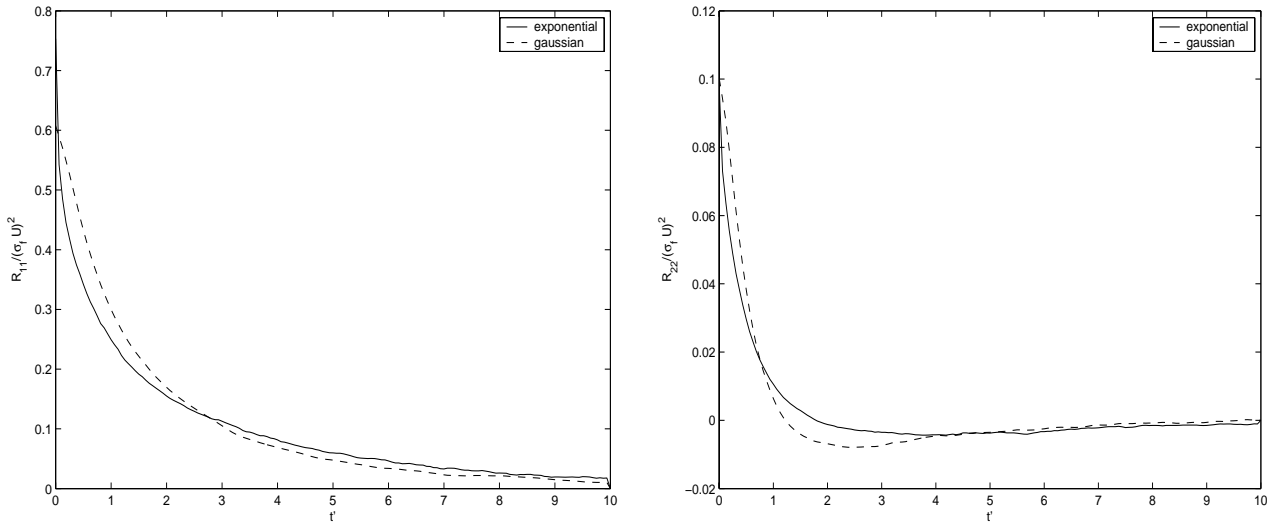


Figure 10: The dimensionless functions $R_{11}(t')/(\sigma_f U)^2$ (left panel) and $R_{22}(t')/(\sigma_f U)^2$ (right panel).

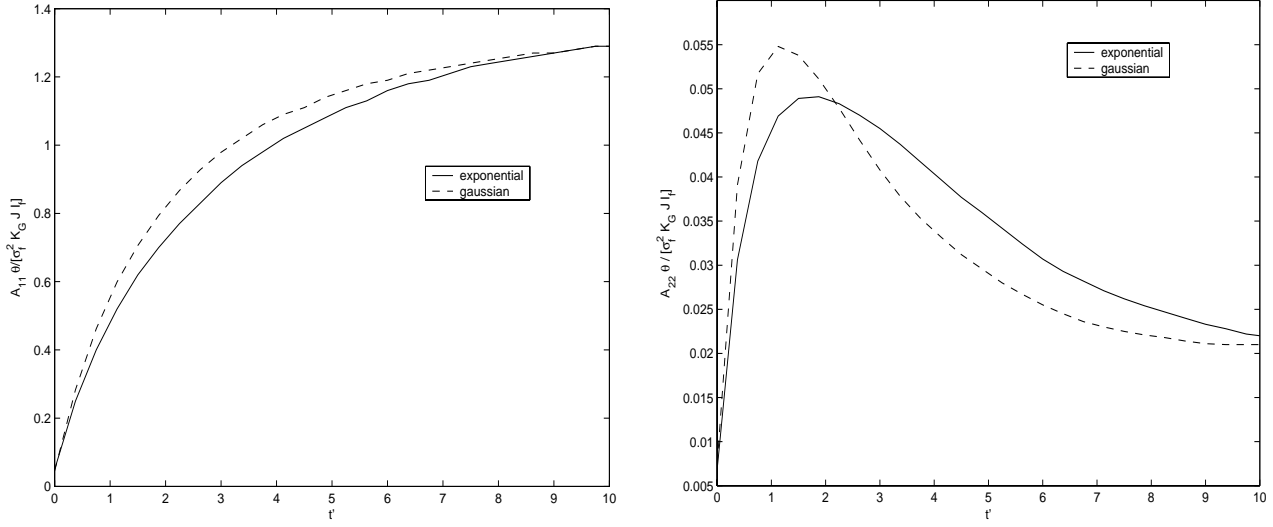


Figure 11: The dimensionless functions $A_{11}(t')\theta/(\sigma_f^2 K_G J I_f)$ (left panel) and $A_{22}(t')\theta/(\sigma_f^2 K_G J I_f)$ (right panel).

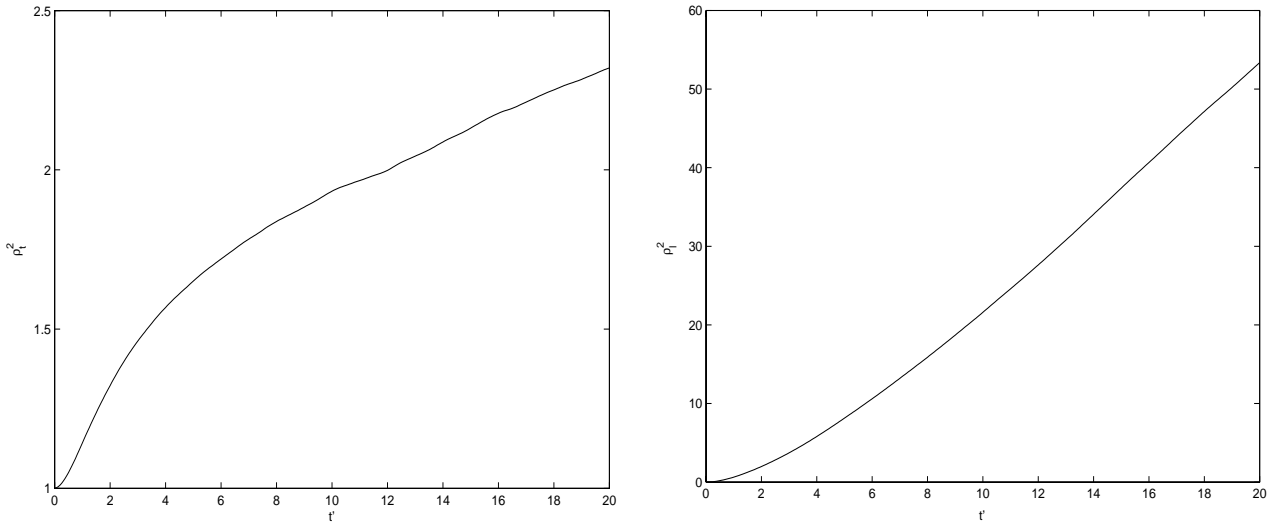


Figure 12: The mean square separation for two particles \mathbf{X} and \mathbf{Y} started at $(0,0,0)$ and $(0,0,1)$, respectively. In the left panel, the transverse mean square separation is presented, and in the right panel the longitudinal mean square separation is shown.

Important Lagrangian statistical characteristic is the mean square separation for two particles. Let $\mathbf{X}(t') = (X_1(t'), X_2(t'), X_3(t'))$ and $\mathbf{Y}(t') = (Y_1(t'), Y_2(t'), Y_3(t'))$ be the Lagrangian trajectories of two particles initially separated by a vector r_0 . The mean square separation $\rho^2(t')$ is defined as

$$\rho^2(t') = \langle (Y_1 - X_1)^2 + (Y_2 - X_2)^2 + (Y_3 - X_3)^2 \rangle.$$

Hence $\rho^2(t') = \rho_l^2(t') + \rho_t^2(t')$ where $\rho_l^2(t') = \langle (Y_1 - X_1)^2 \rangle$, and $\rho_t^2(t') = \langle (Y_2 - X_2)^2 + (Y_3 - X_3)^2 \rangle$ are the longitudinal and transverse mean square separations, respectively.

We show the functions $\rho_l^2(t')$ (left panel) and $\rho_t^2(t')$ (right panel) in Figure 12. Clearly, for sufficiently large time t' the two particles move independently, so we can expect that $\rho^2(t') = 2(D_l + D_t)t'$, according to classical dispersion law where D_l and D_t are the longitudinal and transverse diffusion coefficients, respectively. However for smaller times, the motion of two particles is correlated, and the dependence of $\rho_l^2(t')$ and $\rho_t^2(t')$ on t' is not linear. From the results presented in Figure 12 it can be estimated that the linear law is true approximately after $t' = 10$. For times $t' < 10$, the longitudinal dispersion is superdiffusional $\rho_l^2(t') = C_l t'^{1.4}$ with $C_l = 0.85$. More complicated is the structure of the transverse dispersion. There is a time interval $t' < 2$ where $\rho_t^2(t')$ seems to follow a linear behaviour, and then it switches to the subdiffusional behaviour in $2 \leq t' \leq 10$:

$$\rho_t^2(t') = 1.32 + C_t(t' - 2)^{0.7} \quad (6.2)$$

with $C_t = 0.145$. This agrees well with the behaviour of the Lagrangian correlation functions presented in Figure 10, right panel. Indeed, it suggests that the first time interval of rapidly decaying correlation corresponds to the interval of linear behaviour of $\rho_t^2(t')$, i.e., the diffusion regime is reached. Then, when the negative correlation reaches its maximum (about $t' = 2$), the trapping of particles results in the change of the function $\rho_t^2(t')$ from the linear behaviour, to the subdiffusional regime (6.2).

7. Conclusions and Discussion

Stochastic numerical simulation technique for flow simulation through a 3D statistically isotropic porous media is developed without small perturbation assumptions. The hydraulic conductivity is modelled as an isotropic random field with a lognormal distribution and prescribed structure of the spectral functions. It is sampled by a Monte Carlo method based on a randomized spectral representation. The Darcy and continuity equations with the random hydraulic conductivity are solved numerically, using the successive over relaxation method in order to extract statistical characteristics of the flow. Hybrid averaging is used: we combine spatial and ensemble averaging to get efficient numerical procedure. The method proposed enables us to predict the applicability of the first order approximation model derived under the assumption of small hydraulic conductivity fluctuations. Calculations of the longitudinal and transverse dispersions, the dispersivity, and the Lagrangian correlation functions have been carried out to extract the main statistical features of the flow. In particular, the calculations predict a subdiffusional behaviour of the transverse dispersion, and superdiffusional behaviour of the longitudinal dispersion.

It should be noted that the calculations take a lot of computer time since the stochastic PDE is solved repetitively for many independent samples of the hydraulic conductivity

field with the subsequent ensemble averaging to evaluate the desired statistical characteristics of the solution. A reasonable alternative would be a spatial averaging, but to make this approach realistic, the random field must have good ergodic properties. We applied a hybrid averaging by combining the ensemble and spatial averaging which has considerably decreased the cost of the algorithm. However we have not included here a detailed analysis of the ergodic properties of the randomized spectral models in 3D case; preliminary estimations show that the number of harmonics should be increased simultaneously with the refinement of the mesh used in the finite-difference method. This analysis will be presented in the forthcoming paper.

References

- [1] Rachid Ababou, Dennis McLaughlin, Lynn W. Gelhar, and Andrew F. B. Tompson. Numerical Simulation of Three-Dimensional Saturated Flow in Randomly Heterogeneous Porous Media. *Transport in Porous Media*, **4**, 549-565, 1989.
- [2] Bark, A.A., L.W. Gelhar, A.L. Gutjahr, and J.R. MacMillan. Stochastic analysis of spatial variability in subsurface flows,1, Comparison of one- and three- dimensional flows. *Water Resour. Res.*, **14**(2), 263-271, 1978.
- [3] Bear, J., Dynamics of Fluids in Porous Media. American Elsevier, New York, 1972.
- [4] Alberto Bellin, Paolo Salandin, and Andrea Rinaldo. Simulation of dispersion in heterogeneous porous formations: statistics, first-order theories, convergence of computations. *Water Resour. Res.*, **28**(9), 2211-2227, 1992.
- [5] Chin, D.A., and T. Wang. An investigation of the validity of the first-order stochastic dispersion theories in isotropic porous media. *Water Resour. Res.*, **28**(6), 1531-1542, 1992.
- [6] Dagan G. Solute transport in heterogeneous porous formations. *J. Fluid Mech.*, **145**, 151-177, 1984.
- [7] G. Dagan. A note of the higher-order corrections of the head covariances in steady aquifer flow. *Water Resour. Res.*, **21**, 573-578, 1985.
- [8] G. Dagan. Flow and Transport in Porous Formation. Springer-Verlag. Berlin, Heidelberg, 1989.
- [9] F.-W. Deng and J.H. Cushman. On higher-order corrections to the flow velocity covariance tensor. *Water Resour. Res.*, **31**, 1659-1672, 1995.
- [10] Freeze R.A. A stochastic-conceptual analysis of groundwater flow in non-uniform, homogeneous media. *Water Resour. Res.* **11**(5), 725-741, 1975.
- [11] Gelhar L.W., Gutjahr A.L. and Naff R.L. Stochastic analysis of macro-dispersion in a stratified aquifer. *Water Resour. Res.*, **19**, 161-180, 1979.
- [12] Gelhar, L.J., and C.L. Axness. Three-dimensional stochastic analysis of macrodispersion in aquifers. *Water Resour. Res.*, **19**, 161-180, 1983.

- [13] L.W. Gelhar. Stochastic Subsurface Hydrology. Englewood Cliffs, New Jersey: Prentice Hall, 1992.
- [14] A.E. Hassan, J.H. Cushman, J.W. Delleur. A Monte Carlo assessment of Eulerian flow and transport perturbation models. *Water Resour. Res.*, **34**, 1143-1163, 1998.
- [15] K. Hsu, D. Zhang, S.P. Newman. Higher-order effects on flow and transport in randomly heterogeneous porous media. *Water Resour. Res.*, **32**, 571-582, 1996.
- [16] V.P. Iljin. Finite difference and finite volume element methods for elliptic equations. Institute of Comp. Math. and Math. Geophysics, Russian Academy of Sciences, Siberian Branch, Novosibirsk, 2001 (in Russian)
- [17] Kraichnan R.H. Diffusion by a random velocity field. *Phys. Fluids* (1970), **13**, 1, 22-31.
- [18] P. Kramer, O. Kurbanmuradov, and K. Sabelfeld. Extensions of Multiscale Gaussian random field simulation algorithms. *J. Com. Physics*, in press.
- [19] Kurbanmuradov O., Sabelfeld K., Smidts O. and Vereecken H. A Lagrangian stochastic model for the transport in statistically homogeneous porous media. *Monte Carlo Methods and Applications*, **9** (2003), N 4, 341-366.
- [20] O.A. Kurbanmuradov. Weak convergence of randomized spectral models of Gaussian random vector fields. *Bull. Nov. Comp. Center, Nim. Anal.*, **4** (1993), 19-25.
- [21] O. Kurbanmuradov, K. Sabelfeld and D. Koluhin. Stochastic Lagrangian models for two-particle motion in turbulent flows: Numerical Results *Monte Carlo Methods and Applications*, **3**(1997), 3, 199-204.
- [22] Matheron and de Marsily. Is transport in porous media always diffusive? A counter example. *Water Resour. Res.*, **16**(5), 901-917, 1980.
- [23] A.S. Monin and A.M. Yaglom. *Statistical Fluid Mechanics: Mechanics of Turbulence*, Volume 1,2. The M.I.T. Press, 1981.
- [24] R.L. Naff and A.V. Vecchia. Stochastic analysis of three-dimensional flow in a bounded domain. *Water Resour. Res.*, **22**, 695, 1986.
- [25] F. Poirion and C. Soize. Numerical methods and mathematical aspects for simulation of homogenous and non homogenous Gaussian vector fields. In Paul Kree and Walter Wedig, editors, *Probabilistic methods in applied physics*, volume 451 of *Lecture Notes in Physics*, pages 17-53. Springer-Verlag, Berlin, 1995.
- [26] René A. Carmona, Stanislav A. Grishin, and Stanislav A. Molchanov. Massively parallel simulations of motions in a Gaussian velocity field. In *Stochastic modelling in physical oceanography*, volume 39 of *Progr. Prob.*, pages 47-68. Birkhäuser Boston, Boston, 1996.
- [27] Y. Rubin and G. Dagan. Stochastic Analysis of Boundaries Effects on Head Spatial Variability in Heterogeneous Aquifers, 1. Constant Head Boundary. *Water Resour. Res.*, **24**(10), 1689-1697, 1988.

- [28] Y. Rubin and G. Dagan. Stochastic Analysis of Boundaries Effects on Head Spatial Variability in Heterogeneous Aquifers, 2. Impervious Boundary. *Water Resour. Res.*, **25**(4), 707-712, 1989.
- [29] Karl Sabelfeld and Dmitry Kolyukhin. Stochastic Eulerian model for the flow simulation in porous media. *Monte Carlo Methods and Applications*, **9**(2003), 3, 271-290.
- [30] K.K. Sabelfeld. Monte Carlo Methods in Boundary Value Problems. Springer, New York – Heidelberg – Berlin, 1991.
- [31] K.K. Sabelfeld and O.A. Kurbanmuradov. Two-particle stochastic Eulerian-Lagrangian models of turbulent dispersion. *Mathematics and Computers in Simulation*. **47**(1998), 2-5, 429-440.
- [32] H. Schwarze, U. Jaekel and H. Vereecken. Estimation of Macrodispersion by Different Approximation Methods for Flow and Transport in Randomly Heterogeneous Media. *Transport in Porous Media*, **49**(2001), 2, 267-287.
- [33] H. Sigurgeirsson and A. M. Stuart. A model for preferential concentration. *Phys. Fluids*, **14**(12), 4352–4361, 2002.
- [34] L. Smith and R.A. Freeze. Stochastic Analysis of Steady State Groundwater Flow in a Bounded Domain, 1. One-Dimensional Simulation. *Water Resour. Res.*, **15**(3), 521-528, 1979.
- [35] L. Smith and R.A. Freeze. Stochastic Analysis of Steady State Groundwater Flow in a Bounded Domain, 2. Two-Dimensional Simulation. *Water Resour. Res.*, **15**(6), 1543-1559, 1979.
- [36] D. J. Thomson. Particle pair in kinematic simulations. Technical report, Meteorol. Office, June 13 2003. Turbulence and diffusion note. **289**.
- [37] Andrew F.B. Tompson, A.F.B., Rachid Ababou, and Lynn W. Gelhar. Implementation of the three-dimensional turning bands random field generator. *Water Resour. Res.*, **25**(10), 2227-2243, 1989.
- [38] Tompson, A.F.B., and L.W. Gelhar. Numerical simulation of solute transport in tree-dimensional randomly heterogeneous porous media. *Water Resour. Res.*, **26**(10), 2541-2562, 1990.
- [39] Dongxiao Zhang and Zhiming Lu. An efficient, high-order perturbation approach for flow in random porous media via Karhunen-Loeve and polynomial expansions. *Journal of Comp. Physics*, **194**, 773-794, 2004.